Deep Resources Engineering 1 (2024) 100006

Contents lists available at ScienceDirect

Deep Resources Engineering

journal homepage: www.keaipublishing.com/en/journals/deepre/

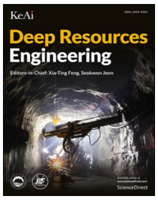

Field observations and interpretation of extensional fracture in hard rock surrounding deep underground openings

Charlie C. Li

NTNU Norwegian University of Science and Technology, Trondheim, Norway

ARTICLE INFO

Keywords:
Extensional fracture
Rock fracture
Failure criterion
Rock burst
Hard rock

ABSTRACT

Extensional fracturing often occurs in hard rock masses during excavation at depths, for example, >1000 m below the ground surface. Surface-parallel fractures are created in the surrounding rock mass, which is typically subjected to stresses parallel to the free rock surfaces after excavation. These are called extensional fractures because the strains perpendicular to the fracture planes are extensional and the opposite surfaces of each fracture tend to separate from each other as soon as the fracture is created. These fractures predominantly propagate parallel to the maximum principal stress σ_1 in the surrounding rock mass. This study analyses extensional fractures observed during excavations in cut-and-fill mining stopes in a deep metal mine. This analysis explores the process of extensional fracturing during excavation in an undisturbed rock mass. In general, intensive spalling occurred on the roof surfaces immediately after the excavation of the undisturbed rock mass. This spalling terminated after a certain depth of rock failure, while burst sounds intermediately emitted from the surrounding rock mass, indicating that rock fracturing was ongoing at depth. In the subsequent cutting slices, the spacing between the extensional fractures decreased with increasing mine-out space in the stope. An extensional fracturing criterion was proposed based on microscopic observations of microcrack development in the rock in response to applied stress. The crack initiation and extensional fracturing processes are associated with two critical extensional strains which are related to the secondary stress state in the position. In areas close to the free rock surface where $\sigma_3 = 0$, the stress for crack initiation is $(\sigma_1+\sigma_2) = 0.4\sigma_c$, whereas the stress for extensional fracturing is $(\sigma_1+\sigma_2) = 0.8\sigma_c$.

1. Introduction

Extensional fracturing, exhibited as spalling and slabbing, is the failure mode most commonly seen during excavation in a hard rock mass [2,3,7,8,16,17,18]. Strain burst events are often related to extensional fracturing. The phenomenon of extensional fracturing has also been observed in laboratory rockburst tests [4,12,14]. In underground excavation, the fractures in the near field of an opening excavated in a hard rock mass are usually extensional even though all the in situ rock stresses are compressive. Based on field and laboratory observations, it is believed that the maximum principal stress for extensional fracturing is lower than the required stress in the Mohr–Coulomb and Hoek–Brown failure criteria. Current studies of extensional fractures in hard rock are limited to qualitative descriptions, and no criterion to quantitatively describe extensional fracturing has been published to date.

The main aim of this study is to demonstrate the phenomenon of extensional fracturing observed in underground excavations in highly stressed hard rock masses. Most of the excavation examples presented in this paper are from a deep metal mine that employed the cut-and-fill mining method. In a cut-and-fill mining stope, it is possible to observe not only the initiation of extensional fractures in the surrounding rock mass, but also the evolution of these fractures when the height of the mine-out space in the stope increases. In addition to observations of extensional fracturing, a quantitative criterion for extensional fracturing is proposed in this paper. This criterion is established based on the knowledge of stress-induced microcracking in rock samples.

2. Observations of extensional fracturing in fields

2.1. Fracture development in cut-and-fill stopes

The cut-and-fill mining method was employed to mine a tabular ore body in a deep metal mine in Europe. The ore was mined by driving a drift of 6 m × 5 m (width × height) along the strike of the ore body, as shown in Fig. 1. Each drift is called a slice of the mine stope in the cut-and-fill mining method. A sublevel mine stope at this site was 25 m high

---

Peer review under responsibility of Editorial Board of Deep Resources Engineering.

https://doi.org/10.1016/j.deepre.2024.100006

Received 8 December 2023; Received in revised form 2 March 2024; Accepted 4 March 2024

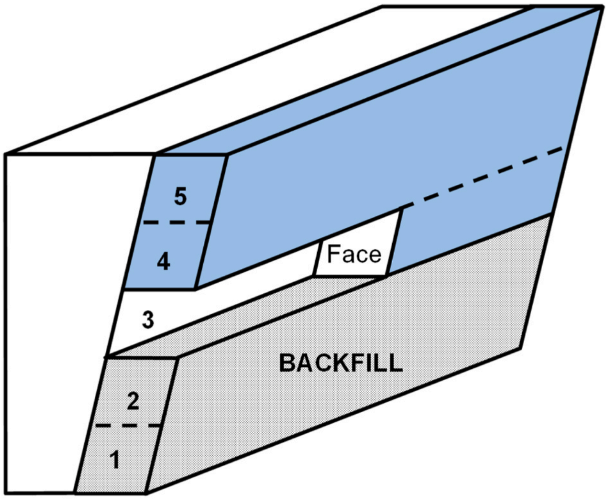

Fig. 1. A sketch illustrating the cut-and-fill mining in a sublevel stope containing five cut slices.

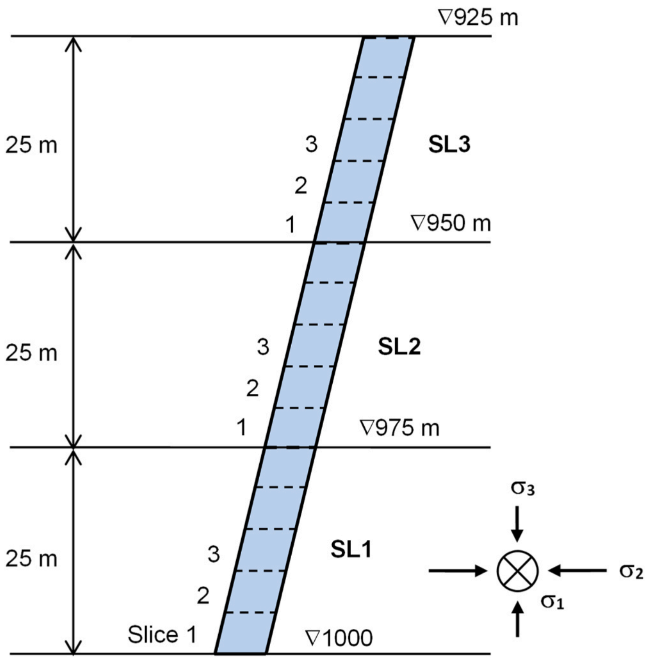

Fig. 2. A sketch illustrating sublevel stopes SL1, SL2, and SL3.

and contained five slices. The cuts always started at the bottom of each stope. After the bottom slice (i.e. the first slice) was mined, it was backfilled with waste rock and tailing sands. The second slice was then excavated standing on the backfilled first slice. This mining cycle was repeated until all five cut slices were excavated. Using this mining method, the roof of the previous slice was exposed on the excavation face of the current slice, thus revealing the fractures in the roof of the previous slice. In this section, the fractures exposed on the faces of some cut slices are described to characterize the fracture development in the surrounding rock mass of the stopes.

The studied stopes were located at a depth of around 1000 m. The mineralization occurs within hydrothermally altered host rocks comprising strongly silicified quartzites with a clear mineral foliation texture. This foliation dips at an angle of 50–75°, which also defines the angles of the hanging and foot walls of the stopes. Sericitic quartzite is the main host rock of the orebody, which is hard, brittle, and originally almost discontinuity-free, except for the mineral foliation texture. The mean value of its uniaxial compressive strength (UCS) was around 120 MPa measured in the laboratory.

Stress measurements reveal that the original maximum and intermediate principal stresses are approximately horizontal in the mine. The maximum principal stress is approximately parallel to the strike of the orebody, while the intermediate principal stress is perpendicular to the strike. These values are approximately 2.3 and 1.4 times the vertical stress, respectively.

The fracturing of the surrounding rock mass in three neighboring sublevel stopes in the mine is presented in this section. Sublevel stope SL1 was located between 1000 m and 975 m below the ground surface, stope SL2 between 975 m and 950 m, and stope SL3 between 950 m and 925 m, as shown in Fig. 2. Each sublevel stope contained five cut slices and mining always commenced in the bottom slice of each stope. Stopes SL1 and SL2 were fully excavated when mining in the bottom slice of SL3 commenced.

2.1.1. *Fractures in the sublevel stope SL1*

The bottom slice, i.e., Slice 1, was first excavated in SL1. The excavation face of this slice was free of stress-induced fractures. Only a few tightly healed geological discontinuities were observed on the face in addition to the sulfide mineral foliations (Fig. 3). Violent spalling occurred on the roof, and intensive noises were recorded immediately after each round of blasting during the excavation of this slice. The roof rock was ejected layer by layer to a depth up to a couple of decimeters (Fig. 4), accompanied by crisp breaking sounds. After a few hours, the superficial spalling terminated, but the burst sounds remained. These burst sounds gradually became lower-pitched and less frequent but more powerful. The burst sounds were emitted from the rock behind the roof and wall surfaces, indicating that rock fracturing was ongoing within the surrounding rock mass. Intensive superficial bursting and rock fracturing in the surrounding rock mass occurred in the first eight hours after excavation blasting; however, sparse bursting events continued to occur even beyond 24 hours after the blasting. The rock fractures developed in the surrounding rock mass were exposed on the excavation faces of the subsequent cut slices in the stope.

Fig. 5 shows the fractures exposed on the excavation face of the crosscut toward Slice 3 of SL1. The rock became fractured into 5–10 cm-thick slabs when the previous two slices were excavated. Fig. 6 shows the fractures exposed on the face of Slice 4. The entire 5 m-high face was fractured, and the observed fractures were much denser than those on the faces of the previous slices, such as those shown in Fig. 5.

2.1.2. *Fractures in the sublevel stope SL2*

The ore in the Slice 1 of SL2 was mined by driving two drifts, labeled as 1–1 and 1–2. Drift 1–1 was excavated first. Fig. 7 shows its excavation face, which contained mineral foliations and a few healed geological discontinuities but no stress-induced fractures.

Drift 1–1 was backfilled after the excavation was completed. Five years later, drift 1–2 was excavated slightly higher than 1–1 so that the fractures in the roof and the wall of 1–1 were exposed during the excavation of 1–2. Fig. 8 shows the fractures in the roof of 1–1, which were horizontal or sub-horizontal, i.e., approximately parallel to the roof surface of 1–1. Fig. 9 shows the fractures in the wall of 1–1, which were sub-parallel to the wall surface of 1–1, with the densest fracturing situated close to the wall surface. This fracturing extended to a depth of approximately 2 m from the wall surface.

Fig. 10 shows the fractures exposed on the excavation face of Slice 2 in SL2. The fractures were sub-horizontal in the lower 2–3 m of the face that formed the roof of the preceding Slice 1. Strain bursts intermittently occurred in the roof of Slice 2, and powerful burst sounds were also intermittently emitted from the rock mass behind the roof surface.

2.1.3. *Fractures in the sublevel stope SL3*

Excavation in the sublevel stope SL3 commenced when the two underlying stopes SL1 and SL2 were completely excavated and backfilled.

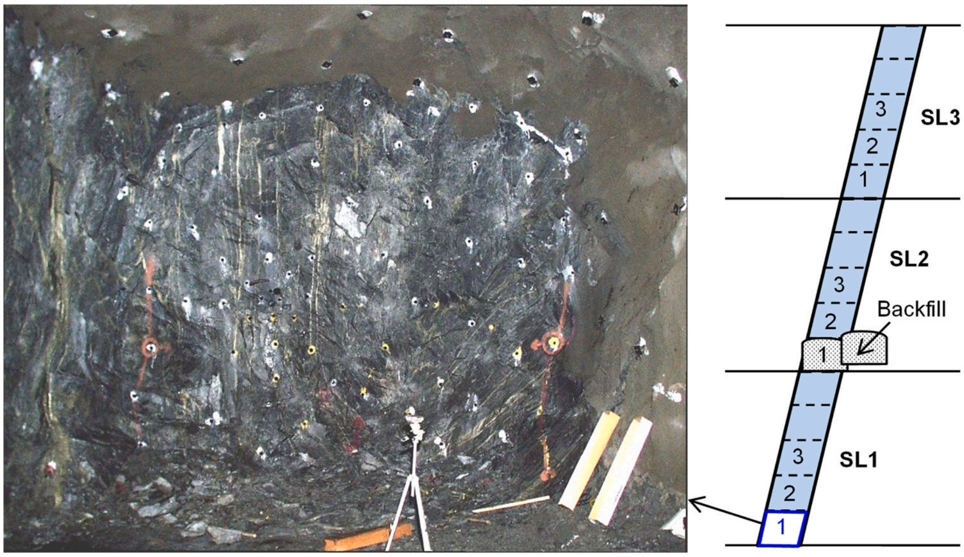

Fig. 3. The excavation face of Slice 1 in SL1.

Fig. 4. Spalling on the roof of Slice 1 in SL1.

Fig. 11 shows the fracturing state of the excavation face of Slice 3 in SL3. Strain bursts rarely occurred during the excavation of this slice due to the heavy pre-fracturing of the surrounding rock mass. However, sparse burst sounds were occasionally emitted from deep locations, indicating that fracturing was ongoing in the surrounding rock mass. The 5 m-high face was densely fractured, and the fractures were perpendicular to the foliation planes and oriented approximately parallel to the intermediate principal stress in the rock mass.

2.2. *Fracturing in a sill pillar*

A 10 m-thick sill pillar was left in a sublevel stope after the three lower slices in the stope had been mined out (Fig. 12). The lower and upper sublevel stopes had been mined out and backfilled. The sill pillar was subjected to heavy fracturing due to the enormous horizontal stress concentration. It was decided that the height of the fourth slice in the stope would be increased to 8 m to mine out the lower part of the sill pillar. The true height of the slice was close to 9 m, leaving an ore layer of slightly more than 1 m thickness at the top after the excavation. The fractures in the sill pillar were exposed on the excavation face of the fourth slice, as shown in Fig. 12. In general, the persistent fractures were predominantly parallel to the in-situ intermediate principal stress that was sub-horizontal in the cross-sectional plane. Vertical fractures also existed between the horizontal fractures. The sill pillar was destressed because of the heavy fracturing. Notably, the excavation of Slice 3 of the

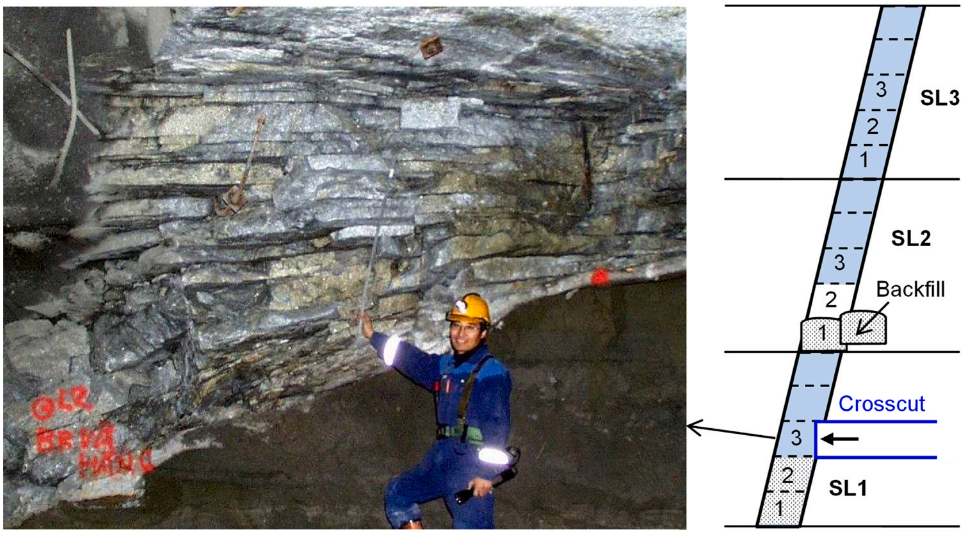

Fig. 5. Fractures exposed on the excavation face of the crosscut toward Slice 3 in SL1.

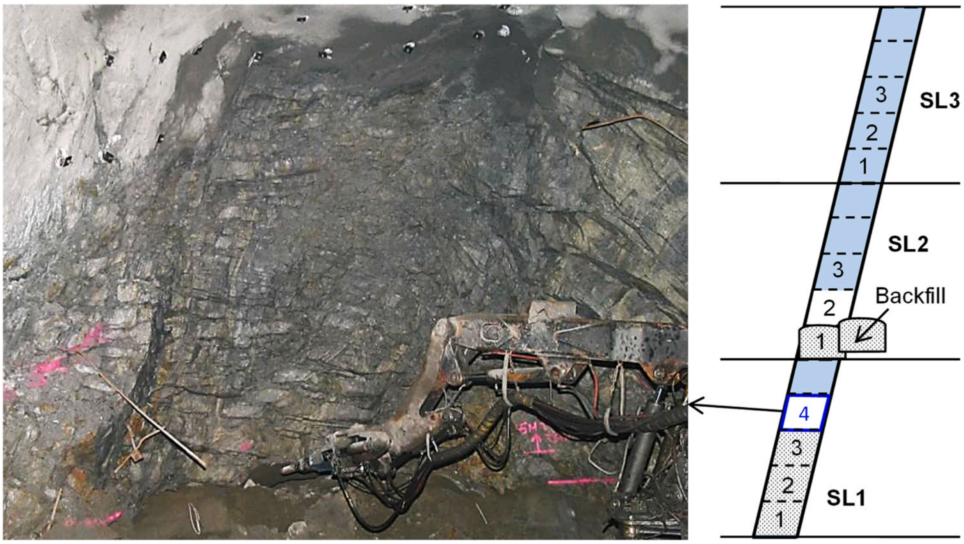

Fig. 6. Fractures exposed on the excavation face of Slice 4 in SL1.

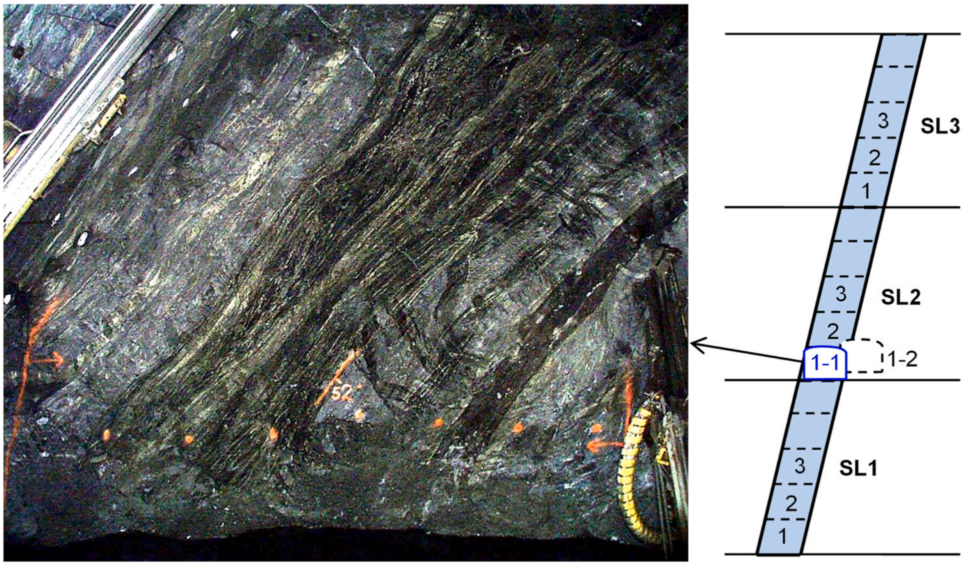

Fig. 7. The excavation face of drift 1–1 in Slice 1 of SL2.

stope was conducted under this heavily fractured roof; however, no major challenges were encountered during the excavation of Slice 3 except abnormal deformations. The rock support system used in the slopte comprised systematic bolting with fully grouted rebar bolts and fiber-reinforced shotcrete. Rehabilitation was required by applying additional bolts and shotcrete during the excavations.

2.3. *Fracturing around strain burst pits*

Fig. 13 shows the fractures within a strain burst pit in the roof of the previous underlying slice. These fractures possibly were created after shotcreting so that falling of the fractured slabs was prevented by the hardened shotcrete layer. The fracture pattern clearly indicates that the failure mode of the rock is extensional, i.e., spalling and slabbing.

Fig. 14 shows the fractures in the rock behind the bottom of a strain burst pit. These fractures were parallel to the burst pit surfaces in the near field of the pit but became parallel to the in-situ stress σ_2 approximately 1 m from the base of the pit. The fractures were tightly spaced due to the extremely high stress concentration. When the current slice was mined, the underlying stopes, which were up to 40 m in height, had been excavated.

2.4. *Fracturing during excavation of a ventilation shaft*

A vertical ventilation shaft was excavated upward at a depth of 950 m in the near field of an old mined-out stope. This shaft was 3 m in diameter and located in hard sericitic quartzite. The rock surrounding the shaft was heavily stressed due to the pre-existing stress concentration around the mined-out stope. Severe strain bursts occurred on the excavation face of the shaft and slabs of a few centimeters in thickness burst from the face immediately after each round of blasting (Fig. 15). The face could be easily advanced a further 1 m simply by scaling down

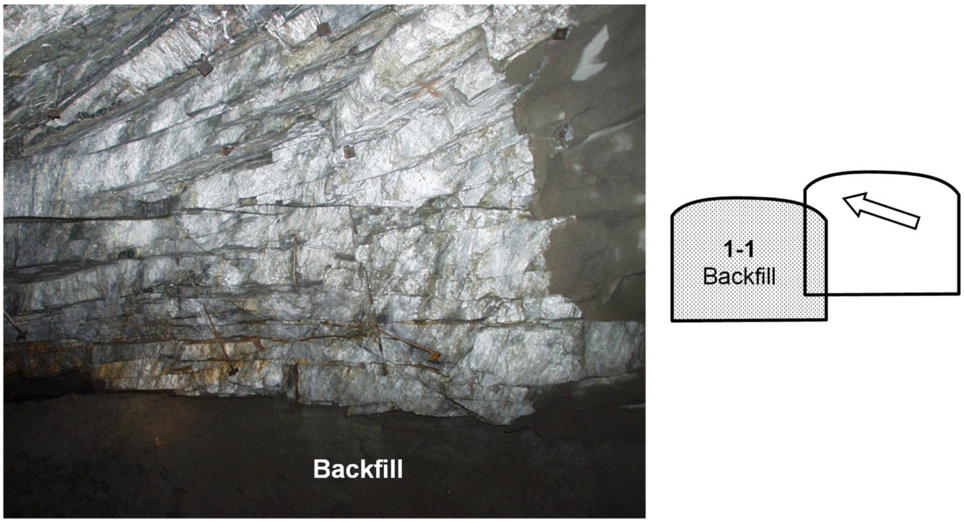

Fig. 8. Stress-induced fractures in the roof rock of Drift 1–1 in the stope SL2.

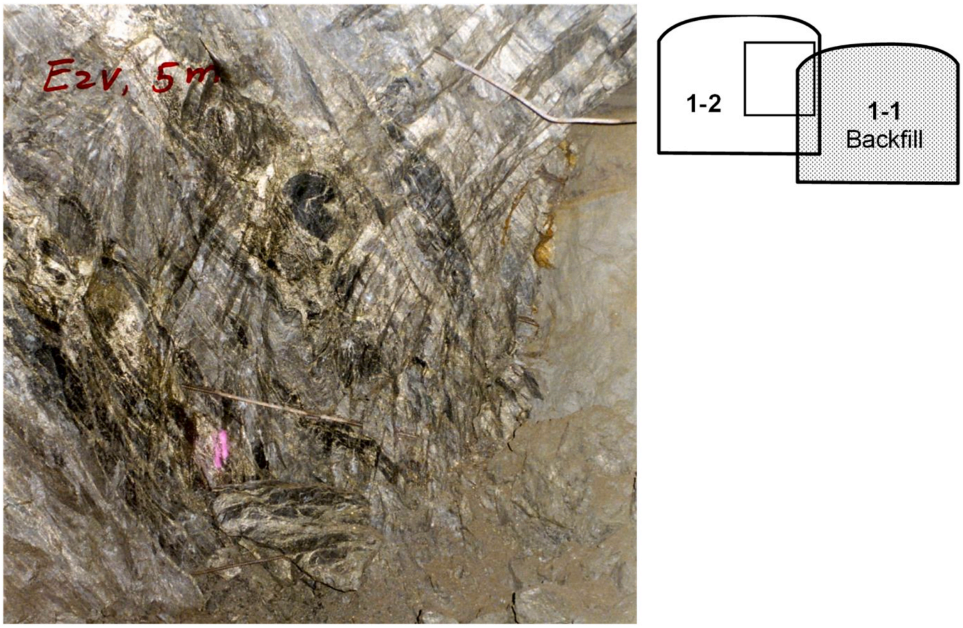

Fig. 9. Stress-induced fractures in the wall of Drift 1–1 in the stope SL2.

the extensionally fractured rock after blasting. De-stressing drilling and pre-bolting of the face were tested to improve the stability of the face; however, the improvements were marginal. The heavy strain bursting forced the excavation to terminate after an advance of 25 m.

2.5. *Fracturing in an ultra-deep gold mine*

Fig. 16 shows extensional fractures exposed on the excavation faces of a deep gold mine in South Africa. The mining stope was at a depth of more than 3000 m. The host rock was a type of quartzite with a UCS between 300 and 400 MPa. Surface-parallel fractures appeared on the benching and side walls of the excavation face, as shown in Fig. 16. Strain bursting, in the form of rock ejection from the excavation face, occurred intermittently in these stopes.

3. Extensional fracture in rock observed in laboratory tests

Wan and Li [15] observed the initiation and propagation of microcracks in hard granite specimens under uniaxial compression. The photos in Fig. 17 show the microcracks observed in thin sections cut from four cylindrical specimens that were vertically loaded at different stress levels. Fig. 17a shows the original microcracks in the granite. The density of the cracks slightly increased at the stress level of 47% of the rock's UCS (Fig. 17b), but significantly increased at the stress level of 80% of the UCS (Fig. 17c). Most of the new cracks initiated at the grain boundaries without orientation preference at those two stress levels. However, when the stress was increased to the level close to the UCS, the cracks predominantly propagated parallel to σ_1 (Fig. 17d). In the post-peak stage, the cracks continued to propagate in the σ_1 direction until the final failure of the specimen. Fig. 18 shows the density variation of the intergranular cracks (i.e., the cracks at the mineral grain boundaries) and intragranular cracks (i.e., the cracks crossing the mineral grains) versus the stress level. These statistics reveal that both the intergranular and intragranular crack densities started to increase at a stress level approximately equal to 50% of the UCS. The density then continued to increase with increasing the applied stress in the pre-peak

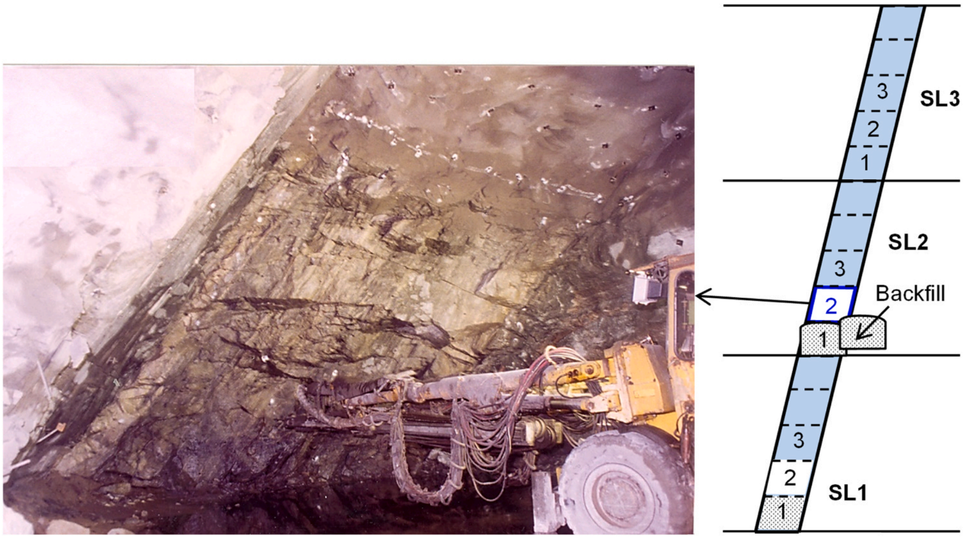

Fig. 10. Fractures exposed on the face of Slice 2 in the stope SL2.

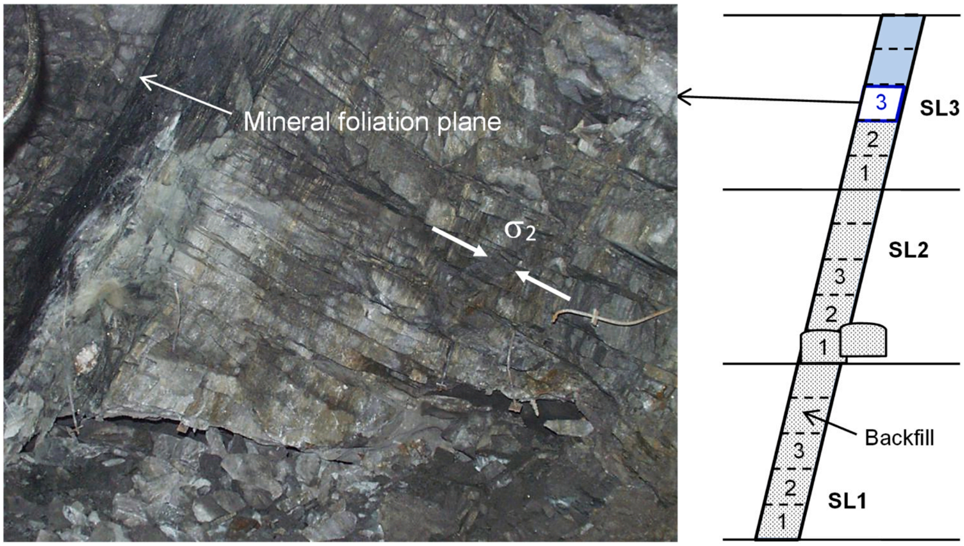

Fig. 11. Fracturing of the face of Slice 3 in the stope SL3.

stage and throughout the entire post-peak stage. Furthermore, the density of the intergranular cracks remained higher than the density of the intragranular cracks during the entire testing period, including both pre-peak and post-peak stages. That implies that the bond between the mineral grains is weaker than the mineral grains in the hard granite. The final failure mode of the granite specimens was splitting in the direction of σ_1, as shown in Fig. 19, i.e., parallel to the dominant propagation direction of the microcracks within the specimen.

4. Criterion for extensional fracture

Martin and Chandler [10] and Martin [9] conducted comprehensive studies of the progressive fracture in Lac du Bonnet granite under compression. They defined three stress levels on the stress-strain curve of the rock: crack initiation stress σ_{ci}, crack damage stress σ_{cd}, and peak strength σ_c, that is, the UCS. The crack initiation stress σ_{ci} is the stress level at which new microcracks start to be generated in the rock. They observed that σ_{ci} was approximately $0.4\sigma_c$ in the Lac du Bonnet granite. The crack damage stress σ_{cd} is the stress level at which unstable crack propagation commences. It was found that σ_{cd} was approximately $0.8\sigma_c$ in the Lac du Bonnet granite.

Li and Nordlund [5] monitored the variation of the acoustic emission (AE) in granite specimens when the specimens were loaded under uniaxial compression at different stress levels and the stress at each level was held unchanged for one hour. Fig. 20 shows the detected AE events in one of the specimens on which the applied stresses were held at $0.3\sigma_c$, $0.5\sigma_c$, $0.78\sigma_c$, and approximately σ_c. Every AE record corresponded to a microcracking event in the specimen. No AE events were detected during the stress holding at the level of $0.3\sigma_c$ (Fig. 20a). AE continued to occur at the level of $0.5\sigma_c$ during the entire stress holding period of one hour (Fig. 20b). At this stress level, the AE event rate attenuated with time and only a few AE events occurred at the end of the one-hour holding period. At the level of $0.78\sigma_c$ (Fig. 20c), the AE rate also attenuated with time during the holding period, but the rate apparently was much higher than at the level of $0.5\sigma_c$. Furthermore, it was still a good number of AE events at the end of the one-hour holding period. That implied that relatively intensive microcracking was occurring during the entire holding period at the level of $0.78\sigma_c$. At the level close to σ_c (Fig. 20d), the AE rate accelerated with the elapse of the holding time, corresponding to accelerated microcracking in the rock. The

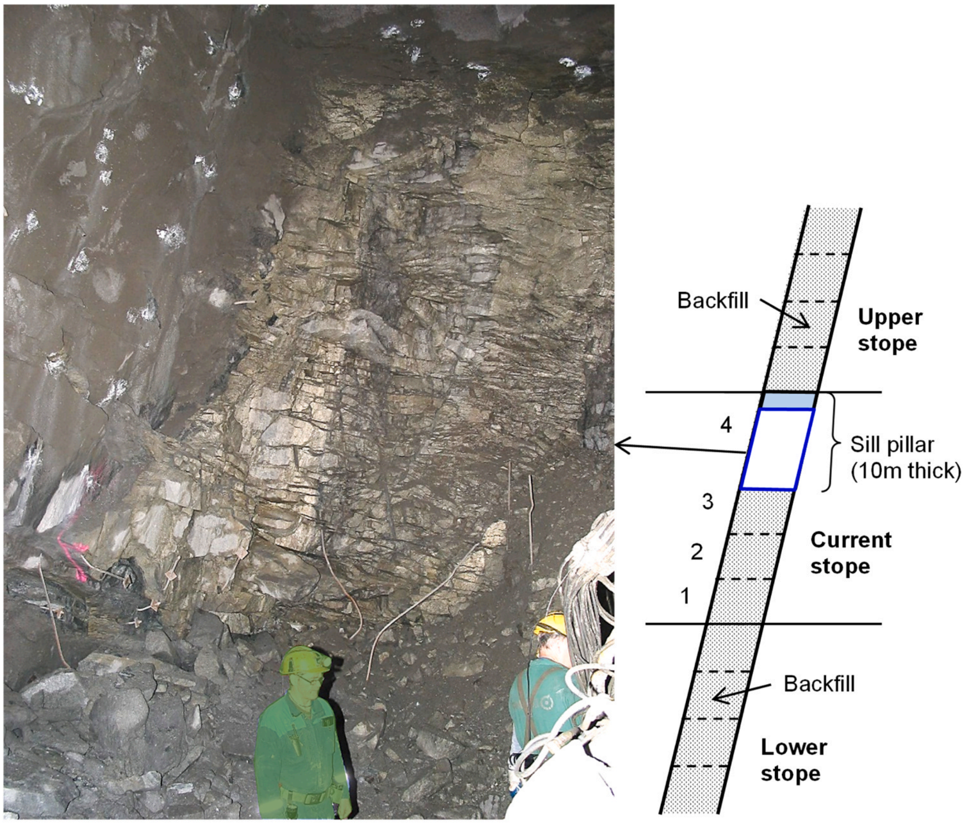

Fig. 12. Sub-horizontal fractures in the 10 m-thick sill pillar in a cut-and-fill stope at a depth of 1000 m.

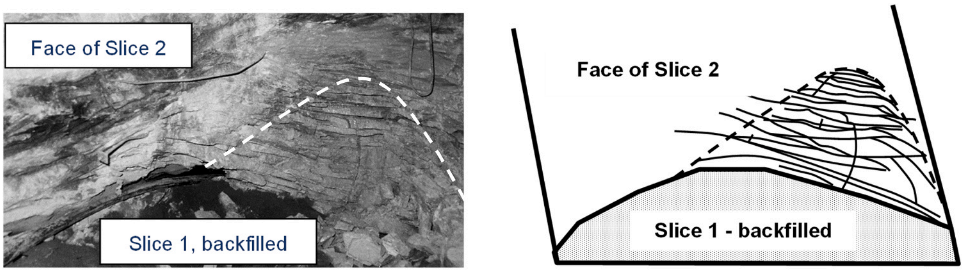

(a) (b)

Fig. 13. The tightly spaced fractures behind the bottom of a strain burst: (a) photo and (b) sketches of the fractures.

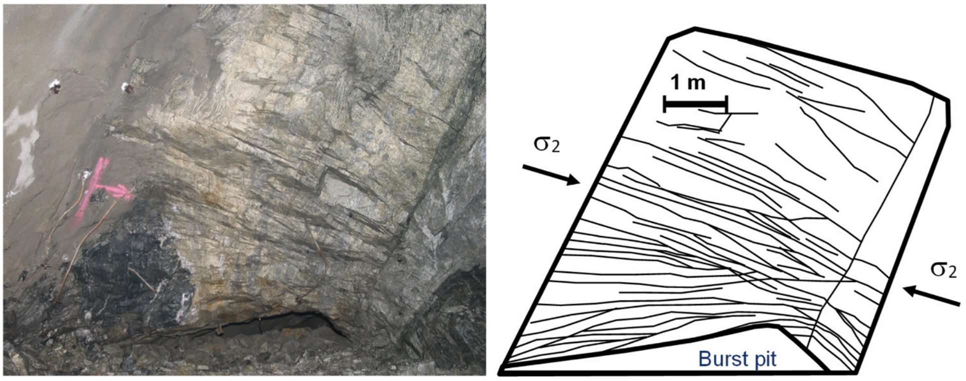

(a) (b)

Fig. 14. Fractures mapped on the excavation face of a cut-and-fill mining stope.

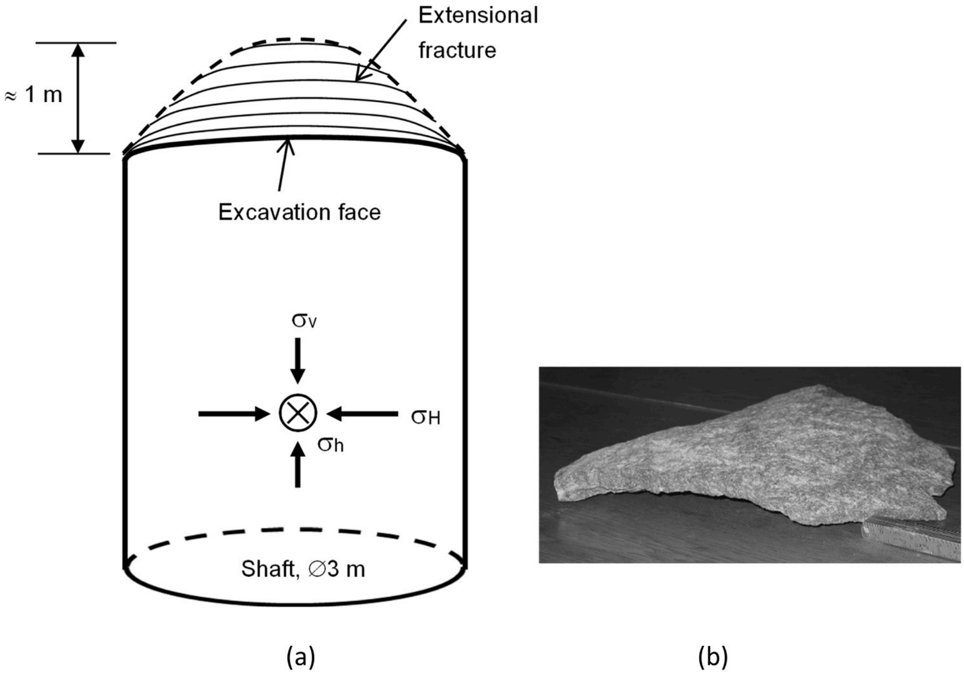

Fig. 15. Extensional fractures behind the excavation face of a vertical ventilation shaft: (a) a sketch illustrating the extensional fractures, and (b) a rock slab that was scaled down from the shaft's excavation face.

specimen finally failed after approximately 4 minutes of holding.

Based on the microcrack observations in Fig. 17, the microcrack statistics in Fig. 18 and the AE monitoring results in Fig. 20, It is inferred that new microcracks initiate in all orientations, that is, without orientation preference, in the stress levels from σ_{ci} to σ_{cd}. However, the microcracks propagate in the direction of the applied stress σ_1 when the applied stress is beyond the crack damage stress σ_{cd}. Therefore, σ_{cd} is the strength of extensional spalling and slabbing fracture in hard rock.

Both field observations and laboratory tests have confirmed that extensional fractures initiate in hard and brittle rocks when the compressive stress is lower than the strength of shear failure. Stacey [13] proposed a simple descriptive criterion for extensional fracture, which stated that extensional fracturing would initiate when the extensional strain reached a critical value. He did not tell how the critical extensional strain threshold would be determined. Shen and Barton [11] postulated that the critical extensional strain under compression would be identical to the maximum tensile strain under tension. The author of this paper compared the extensional strains at σ_{ci} in compression tests with the maximum tensile strains in tensile tests for a few types of hard rocks. He found that the extensional strain at σ_{ci} in the compression tests were higher than the maximum tensile strain in the direct tensile tests. How to determine the critical extensional strain under compression remains unsolved at present.

As stated above, the crack initiation occurs at $\sigma_{ci} = 0.4\sigma_c$ under uniaxial compression. The critical minor strain for crack initiation is thus obtained, according to Hooke's law, as:

$$\varepsilon_{3,ci} = -\frac{1}{E}0.4\nu\sigma_c \tag{1}$$

Similarly, the critical minor strain for extensional fracture at $\sigma_{cd} = 0.8\sigma_c$ is obtained as:

$$\varepsilon_{3,cd} = -\frac{1}{E}0.8\nu\sigma_c \tag{2}$$

In three-dimensional stress state, the minor strain in the direction of the minor principal stress σ_3 is expressed, according to Hooke's law, as:

$$\varepsilon_3 = \frac{1}{E}[\sigma_3 - \nu(\sigma_1 + \sigma_2)] \tag{3}$$

The critical values of ε_3 for crack initiation and extensional fracture should be the same as the values in uniaxial stress state, respectively. By letting the right sides of (1) and (3) be equal, the criterion for crack initiation is then obtained as:

$$\sigma_3 - \nu(\sigma_1 + \sigma_2) = -0.4\nu\sigma_c$$

The criterion for extensional fracturing is obtained, by letting the right sides of (2) and (3) be equal, as:

$$\sigma_3 - \nu(\sigma_1 + \sigma_2) = -0.8\nu\sigma_c$$

The above two criteria are written in a general form as:

$$\frac{\sigma_1 + \sigma_2}{\sigma_c} = \frac{1}{\nu}\frac{\sigma_3}{\sigma_c} + k \tag{4}$$

where $k = k_{ci} = 0.4$ for crack initiation and $k = k_{cd} = 0.8$ for extensional fracture (i.e., spalling and slabbing).

The criterion for crack initiation was qualitatively sketched as an S-curve in the σ_1–σ_3 space by Diederichs [1]. The exact shape of the curve is not known to date. Eq. (4) is a general criterion for both crack initiation and extensional fracture, which is derived based on an assumption that the crack initiation and extensional fracture are caused by the extensional strain and the critical extensional strain is the same under uniaxial and triaxial stress states. The validity of the criterion needs experimental verifications in the future. The criterion is illustrated by two blue lines in Fig. 21. The thin blue line represents the limit for crack initiation, and the thick blue line for the onset of extensional fracture. The laboratory short-term rock strength is also plotted by a thick black line in the figure.

5. Conclusions

The field observations and laboratory microscopic observations presented in this study demonstrate that the primary failure mode of

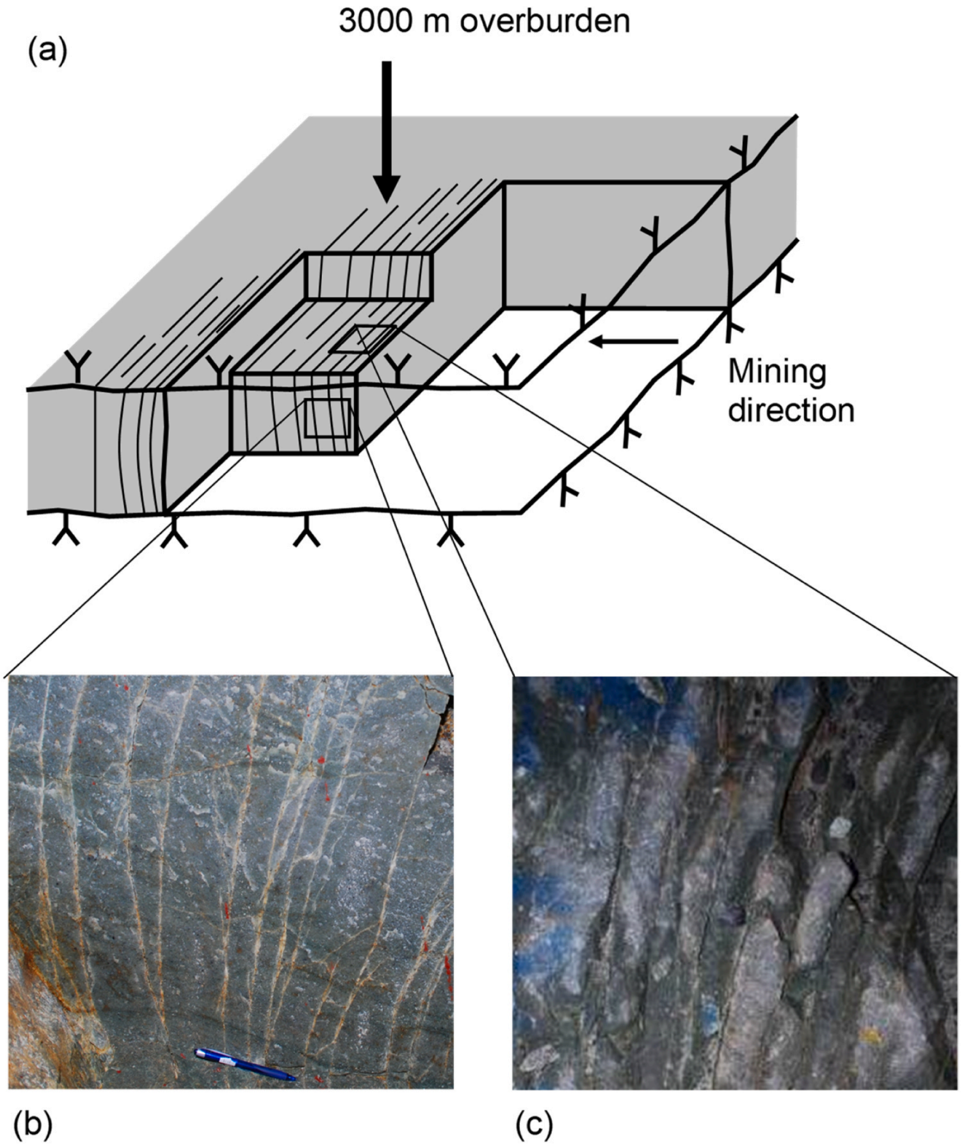

Fig. 16. Extensional fracture in hard rock in an ultra-deep gold mine in South Africa [6].

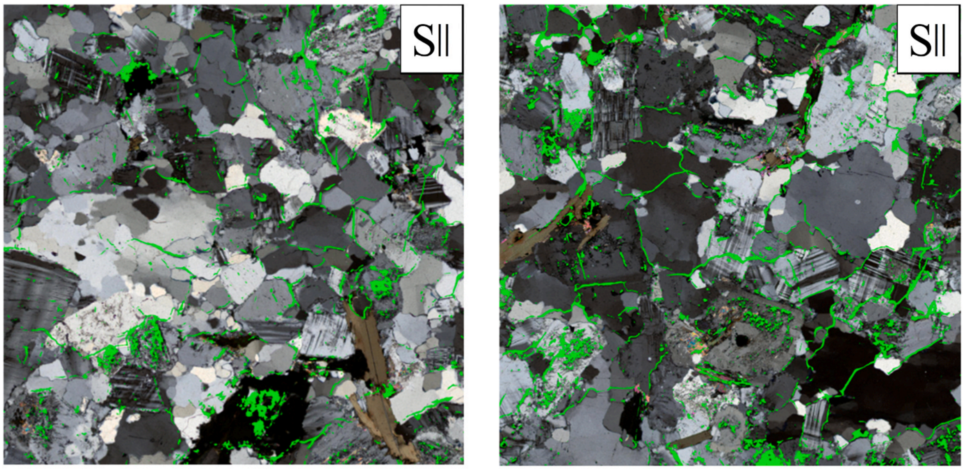

(a) σ_1 = 0 MPa

(b) σ_1 = 47%UCS (pre-peak)

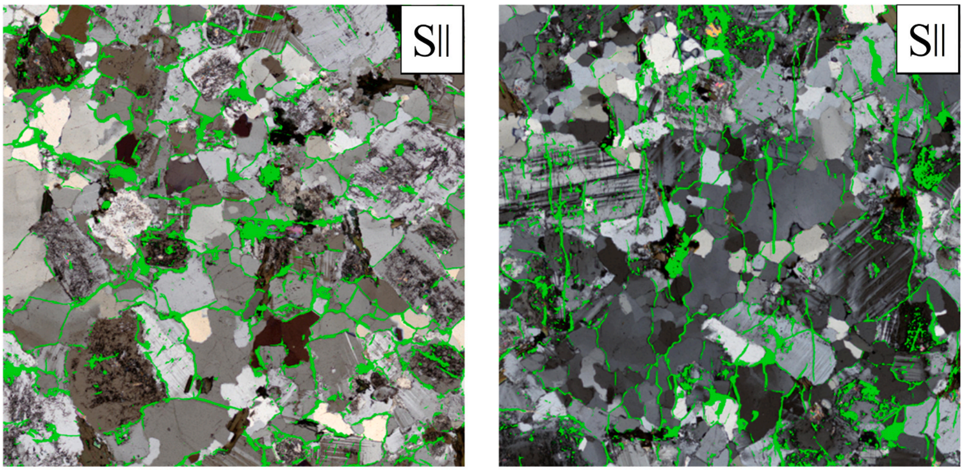

(c) σ_1 = 80%UCS (pre-peak)

(d) σ_1 = UCS

Fig. 17. Microcracks (green-colored) in the thin sections cut in the σ_1 direction of the granite specimens. [15].

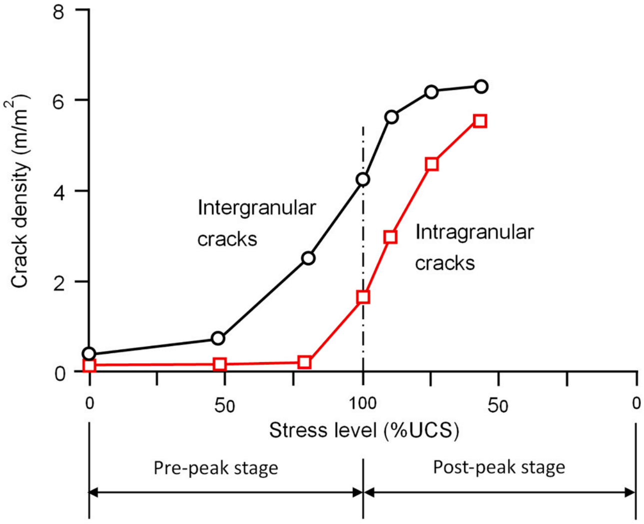

Fig. 18. Statistics describing the microcrack density throughout the loading period of the granite specimens [15].

Fig. 19. The final failure mode of the granite specimen (50 mm in diameter with a length-to-diameter ratio of 2.5).

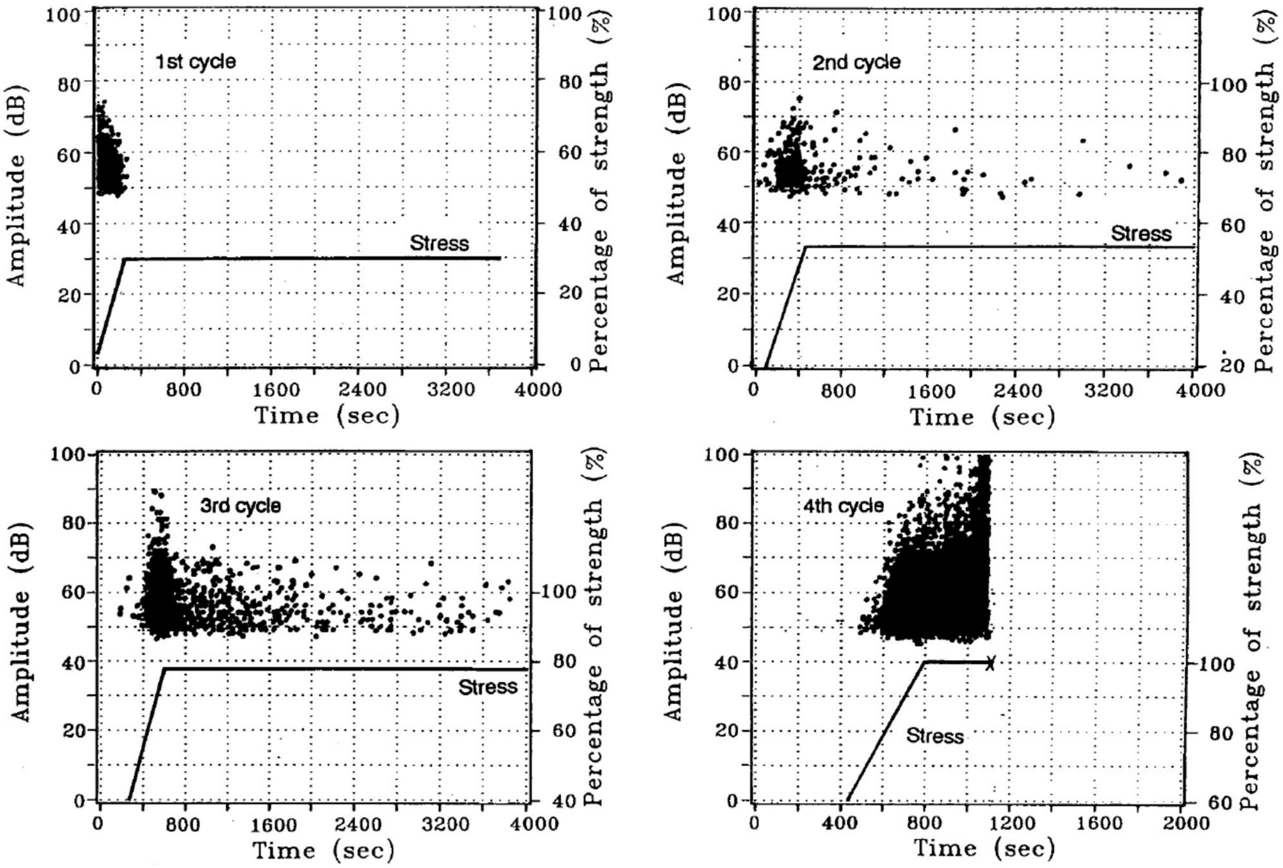

Fig. 20. Acoustic emission in a hard granite specimen under four stress levels of uniaxial compression [5].

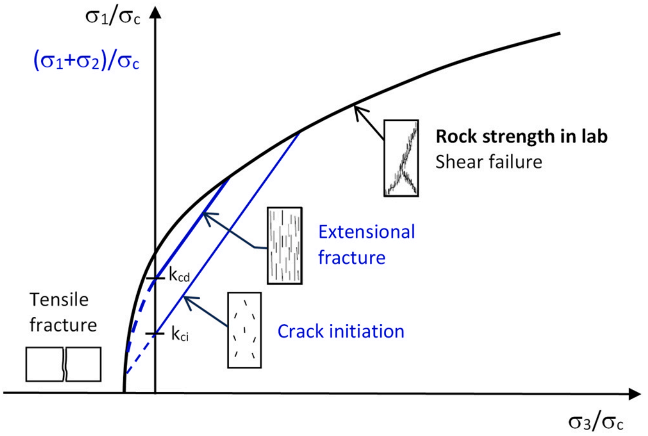

Fig. 21. A diagram illustrating the limits for crack initiation and extensional fracture as well as the laboratory short-term strength of the rock. σ_c is the short-term strength of the rock under uniaxial compression.

hard rock in deep underground settings is extensional fracturing parallel to the contour surfaces of the underground opening. In general, the fracture density is high close to the contour surfaces, and the fracture spacing increases with increasing distance from the opening. The fracture density is directly proportional to the stress concentration in the surrounding rock mass.

In hard rock, new crack initiation begins at the boundaries of hard and strong mineral grains at very low stress levels, e.g., approximately 40% of the UCS under uniaxial compression. The crack propagation has not orientation preference until the stress reaches approximately 80% of the rock strength. Above this stress level, extensional fracture dominates in the σ_1 direction, and finally macroscopic spalling and slabbing fracture occur. A general criterion for crack initiation and extensional fracture is proposed.

Declaration of Competing Interest

The authors declare that there is no conflict of interest.

Acknowledgements

The author is grateful to Boliden for its approval of disclosing some of the field observations of rock fracture presented in this article. It is acknowledged that the article was prepared with the financial support by NTNU Norwegian University of Science and Technology.

References

[1] M.S. Diederichs, Rock fracture and collapse under low confinement conditions, Rock Mech. Rock Eng. 36 (5) (2003) 339–381.
[2] Diederichs, M.S. 2014. When Does Brittle Failure Become Violent? Spalling And Rockburst Characterization For Deep Tunneling Projects. Proceedings of the World Tunnel Congress 2014, Foz do Iguaçu, Brazil. 10p.
[3] Fairhurst, C. and Cook, N.G.W. 1966. The Phenomenon of Rock Splitting Parallel to the Direction of Maximum Compression in the Neighbourhood of A Surface. In: Proceedings of the 1st Congress of the International Society of Rock Mechanics, Lisbon, Vol. I: 687-692.
[4] B.G. He, Q. Tong, X.T. Feng, Q. Jiang, H. Li, Y.H. Li, Z.G. Li, Brittle failure modes of underground powerhouses: an insight based on true triaxial compression tests, Bull. Eng. Geol. Environ. 82 (2023) 153.
[5] C. Li, E. Nordlund, Experimental verification of the Kaiser effect in rocks, Rock Mech. Rock Eng. 26 (4) (1993) 333–351.
[6] C.C. Li, Rockbolting: Principles and Applications, Butterworth-Heinemann, 2017.
[7] F. Li, Q. Zhang, K. Duan, W. Xiang, G. Yu, Investigating the mechanism of splitting failure in deep high sidewall cavern based on complex function and strain gradient, Tunn. Undergr. Space Technol. 132 (2023) 104910.

[8] S.J. Li, X.T. Feng, Z.H. Li, B.R. Chen, C.Q. Chuanqing Zhang, H. Zhou, In situ monitoring of rockburst nucleation and evolution in the deeply buried tunnels of Jinping II hydropower station, Eng. Geol. 137–138 (2012) 85–96.

[9] C.D. Martin, Seventeenth Canadian geotechnical colloquium: the effect of cohesion loss and stress path on brittle rock strength, Can. Geotech. J. 34 (5) (1997) 698–725.

[10] C.D. Martin, N.A. Chandler, The progressive fracture of Lac du Bonnet granite, Int. J. Rock Mech. Min. Sci. Geomech. Abstr. 31 (6) (1994) 643–659.

[11] B. Shen, N. Barton, Rock fracturing mechanisms around underground openings, Geomech. Eng. 16 (1) (2018) 35–47.

[12] L. Shi, C.C. Li, X.W. Zhang, X.T. Feng, Experimental verification of the intrinsic strainburst proneness of various rock types, Bull. Eng. Geol. Environ. 82 (2023) 119.

[13] T.R. Stacey, A simple extensional strain criterion for fracture of brittle rock, Int. J. Rock Mech. Min. Geomech. Abstr. 18 (1981) 469–474.

[14] S.G. Su, L.H. Hu, X.T. Feng, L.B. Yan, G.L. Zhang, S.Z. Yan, B. Zhao, Z.F. Yan, True triaxial experimental study of rockbursts induced by ramp and cyclic dynamic disturbances, Rock Mech. Rock Eng. 51 (2018) 1027–1045.

[15] W.K. Wan, C.C. Li, Microscopic and acoustic interpretations of the physics of rock burst and the difference in fracturing patterns in Class I and Class II rocks, Rock Mech. Rock Eng. 55 (2022) 6841–6862.

[16] P. Xiao, D. Li, G. Zhao, H. Liu, New criterion for the spalling failure of deep rock engineering based on energy release, Int. J. Rock Mech. Min. Sci. 148 (2021) 104943.

[17] P. Xiao, D. Li, G. Zhao, Q. Zhu, Characteristics and mechanism of rockburst at five deep gold mines in Jiaodong Peninsula of China, Int. J. Rock Mech. Min. Sci. 171 (2023) 105574.

[18] Y.X. Xiao, X.T. Feng, S.J. Li, G.L. Feng, Y. Yu, Rock mass failure mechanisms during the evolution process of rockbursts in tunnels, Int. J. Rock Mech. Min. Sci. 83 (2016) 174–181.

Charlie Chunlin Li is a professor of rock mechanics for civil and mining engineering at the Norwegian University of Science and Technology (NTNU) in Norway. Before his academic career at NTNU, he worked as a research associate and an associate professor at Lulea University of Technology, Sweden; as a ground control engineer at Boliden Mineral Ltd., Sweden; and as the chief technical officer in Dynamic Rock Support AS, Norway. His expertise is in stability analyses of underground spaces and ground control. He is a member of the Norwegian Academy of Technological Sciences (NTVA). He was the vice president of Europe 2015–2019 in the International Society for Rock Mechanics and Rock Engineering (ISRM).